JOURNAL OF SOLID STATE CHEMISTRY 68, 340–350 (1987)

Solid-State and Surface Chemistry of Sn-Doped In_2O_3 Ceramics

P. A. COX AND W. R. FLAVELL*

Inorganic Chemistry Laboratory, South Parks Road, Oxford OX1 3QR, United Kingdom

AND R. G. EGDELL

Department of Chemistry, Imperial College, South Kensington, London SW7 2AZ, United Kingdom

Received August 11, 1986; in revised form October 7, 1986

Tin-doped indium oxide (ITO) ceramics prepared by a high-temperature solid-state synthetic procedure have been studied over the composition range 1–6 at.% Sn by X-ray and ultraviolet photoelectron spectroscopy (XPS and UPS) and high-resolution electron energy loss spectroscopy (HREELS). Surface tin enrichment is evident from XPS with a heat of segregation of around -40 kJ mole^{-1}. However, the surface free-carrier concentration probed via the conduction-to-valence band intensity ratio in UPS or the surface plasmon frequency in HREELS is lower than the nominal tin concentration. It is concluded that electrons associated with segregated Sn ions in the topmost surface plane occupy a lone-pair-like *sp* hybrid surface state, while the region immediately below the surface is depleted in free carriers as a result of donor trapping effects and evaporation of tin during preparation. © 1987 Academic Press, Inc.

1. Introduction

Thin films of tin-doped In_2O_3 (ITO) deposited on glass substrates have been shown to reflect electromagnetic radiation almost completely in the infrared, while having high transmittance in the visible region (*1*). This leads to important technological applications as heat-reflecting mirrors, for example, in sodium discharge lamps and solar collectors (*2*). The films have good electrical conductivity, those showing optimum properties usually displaying carrier concentrations of $\sim 1.5 \times 10^{21}$ cm^{-3} at doping levels of 8–15 at. % (*3*). Despite their potential importance, the surface properties of ITO materials have been little studied. In addition, the bulk optical and electrical properties of ITO films tend to be strongly dependent on the method and precise conditions of film production (*4, 5*). It is clear that incomplete attainment of thermal equilibrium during film production is a major cause of these variations (*5*). In the present paper, we use the complementary techniques of X-ray and ultraviolet photoelectron spectroscopy (XPS and UPS) and high-resolution electron energy loss spec-

* Author to whom correspondence should be addressed. Present address: Department of Chemistry, Imperial College, South Kensington, London SW7 2AZ, UK.

0022-4596/87 $3.00
Copyright © 1987 by Academic Press, Inc.
All rights of reproduction in any form reserved.

troscopy (HREELS) to explore the surface properties of ITO ceramics. The study of well-characterized ceramics, having tin doping levels below the solubility limit of ~6 at.% (*3*), was seen as a necessary precursor to further studies of ITO thin films having higher doping levels. The latter will form the subject of a subsequent publication.

The nature of the species contributing to the carrier concentration in ITO is a matter of some controversy. In_2O_3 itself is a semiconductor with a direct band gap of about 3.6 eV (*6, 7*) and an indirect gap of about 2.6 eV (*8*). As prepared, indium oxide is generally somewhat reduced, containing oxygen vacancies, In_2O_{3-x} $(V_O^{\cdot\cdot})_x e'_{2x}$ with $x<0.01$ (*9, 10*). The conductivity is accordingly n-type. Tin is believed to be substitutionally incorporated into the In_2O_3 lattice in ITO. The ambient oxygen pressure during film production seems to be of importance in determining the properties of the resulting materials. In sputtered films prepared at low oxygen pressure, incorporation as Sn^{2+} has been postulated (*1, 11, 12*). Both SnO (*11*) and Sn_3O_4-like (*12*) phases have been suggested; Fan and Goodenough (*13*) propose that formation of the latter is responsible for the film darkening and high electrical resistivity observed in materials prepared under nonequilibrium conditions. It is suggested that at low deposition rates and high deposition temperatures, the atomic mobilities relative to the rate of film growth are high enough for any second phase to be ejected to the surface (*13*). Such a surface enrichment in tin has been observed by XPS (*13, 14*) and depth profiling Auger electron spectroscopy (*1, 14, 15*).

In films prepared under oxygen-rich conditions and at higher substrate temperatures (around 500°C), only Sn^{4+} has been detected by Mössbauer spectroscopy both in the as-grown state and after annealing under reducing conditions (e.g., in the presence of a 1:1 $CO:CO_2$ mixture (*4, 16*)). The donor activity of the Sn dopant is thus attributed to substitutional Sn^{4+} on In^{3+} sites. In such films, an uncontrollable amount of oxygen is introduced into the films during preparation, reducing the conductivity by trapping the free electrons contributed by the donor. The bixbyite structure of In_2O_3 allows for the ready incorporation of oxygen on quasi-oxygen vacancy sites. The effect may be reversed by annealing the films in a reducing atmosphere (*2–4, 16*). In the "reduced" films it is found that, up to doping levels of around 5–6 at.% Sn, each tin atom is electrically active, having donated a conduction electron, $In_{2-\delta}Sn_\delta^{\cdot}O_3e'_\delta$ (*2, 3*). A detailed defect model is developed for these films by Frank and Köstlin (*4*). It is envisaged that while the predominant defects at low oxygen partial pressures are substitutionally incorporated Sn^{4+} ($Sn^{\cdot}$) and oxygen vacancies, $V_O^{\cdot\cdot}$, at higher partial pressures defect clusters are formed, involving interstitial oxide ions which trap the donor electrons. Upon prolonged heat treatment of the films these clusters may nucleate to form a separate SnO_2 phase (*3*).

2. Experimental

Samples containing 1, 4, and 6 at.% Sn were prepared by a coprecipitation method. Weighed quantities of In foil and Sn wire (Johnson Matthey Puratronic) were dissolved in aqua regia made from BDH Analar grade acids. The solution was made alkaline with excess NH_3, and, after boiling for 2 hr, the resulting precipitate was collected and washed. After overnight drying at 400 K, the powdered material was finely ground in an agate mortar and fired for a period of 7–14 days in air at 1270 K in a recrystallized alumina crucible. Following this initial annealing period, the samples were pressed into pellets between optically smooth tungsten carbide disks and were sintered in air for a further period of 4–7

days at 1270 K to yield mechanically robust ceramic disks. A proportion of the pellets was then fired at 1470 K for 4–7 days, and several of these pellets were subjected to an additional firing at 1630 K for 4 days. Thus, the minimum firing period was 11 days, while pellets ultimately heated at the highest temperature of 1630 K were subject to up to 5 weeks of firing at temperatures $\geq$1270 K. We therefore feel confident that thermal equilibrium has been attained at all the temperatures used.

Continuous X-ray powder diffraction profiles were obtained from all the samples using a Philips moving-arm diffractometer. All profiles showed narrow peaks associated with a well-crystallized cubic (*Ia*3) In_2O_3 phase. No peaks due to α-SnO, β-SnO, or Sn_3O_4 phases were observed. However, in some samples (notably those having high nominal concentrations of tin and heated at lower temperatures) small peaks due to a SnO_2 (rutile) phase were apparent. Estimates of the SnO_2 content of the ceramic samples are given in Table I. Our results suggest that the solubility limit of tin in powder samples of In_2O_3 calcined at 1270 K is rather lower than the figure of 6 $\pm$ 2 at.% put forward by Frank *et al.* (*3*) for samples annealed up to this temperature.

TABLE I

TIN DIOXIDE CONTENT OF ITO CERAMICS AS DETERMINED BY XRD

Nominal tin content (at.%)	Firing temperature (K)	Sn in form SnO_2 (at.%)
1	1270	0
	1470	0
	1630	0
4	1270	1–2
	1470	1–1.5
	1630	0
6	1270	5–6
	1470	2–3.5
	1630	0

Lattice parameters for most of the samples were very similar, and were within 0.1% of that of pure In_2O_3. However, parameters for samples containing 6 at.% Sn tended to be slightly larger than those of In_2O_3. This is in accord with the work of Frank and Köstlin (*4*) and is attributed by these authors to the additional repulsion caused by the larger effective charge of the Sn^{4+} ions.

Several ceramic samples were examined by SEM and TEM using a JEOL JEM-2000FX electron microscope. SEM revealed that the samples were well crystallized, the size of the crystallites increasing with sample firing temperature. In samples containing no separate SnO_2 phase (as determined by XRD), TEM using In$K\alpha$ and Sn$K\alpha$ emissions indicated a homogeneous tin content consistent with the bulk nominal doping level. Samples having a significant SnO_2 content showed an inhomogeneous tin distribution, as expected.

Solid-state laser-induced Raman spectra were obtained from the ceramic samples and from pure In_2O_3 using a relatively weak blue line of a krypton laser (20,997.7 cm^{-1}) in order to minimize the intensity of the fluorescent background. The spectrometer employed a Spex Ramalog 5 triple monochromator coupled to a Spex Datamate data acquisition system. Spectra obtained from the ITO samples were not significantly different from those for pure In_2O_3 and showed the Raman-active phonons of the bixbyite structure at typically 467, 498, and 781 cm^{-1}, in good agreement with literature values (*17*).

Electron spectra were measured in an ESCALAB spectrometer (V.G. Scientific, East Grinstead, UK) with facilities for excitation of photoelectron spectra using unmonochromated Al$K\alpha$ or Mg$K\alpha$ X-rays or UV radiation from a noble-gas discharge lamp, as well as with a monochromated electron source for HREELS. The samples, mounted in platinum trays, were cleaned in the preparation chamber of the

spectrometer (base pressure 5×10^{-8} Torr) by annealing overnight at temperatures roughly equal to their final firing temperatures. This was seen as a necessary precaution to minimize the possibility of any further reaction occurring during the cleaning procedures.

Surface cleanliness was monitored by HREEL spectra, which under vacua of $\sim 10^{-10}$ Torr remained free of loss signals due to hydrocarbons or other contaminants for up to 12 hr. Recleaning was routinely carried out overnight. Electron spectra were accumulated in an ORTEC 6240B multichannel analyzer and were transferred to floppy disks for subsequent analysis in a Research Machines Ltd. 380Z microcomputer.

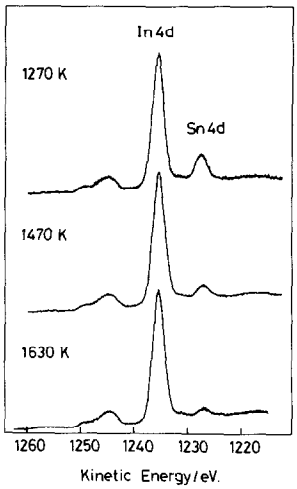

FIG. 2. Examples of Mg$K\alpha$ XPS of ITO ceramics containing 6 at.% Sn, in the metal 4*d* region. Firing temperatures are indicated. Peaks to the left of the main features are due to satellite radiation.

3. Results and Discussion

3.1. X-Ray Photoelectron Spectra

Mg$K\alpha$ excited X-ray photoelectron spectra in the region of the metal 3*d* ionizations are shown in Fig. 1 for pellets containing 1, 4, and 6 at.% Sn. All pellets were calcined at 1270 K. Figure 2 shows three spectra of the metal 4*d* region taken from a sample containing nominally 6 at.% Sn, but calcined at three different temperatures. Following a subtraction of background and satellite structure (*18*), it is possible to derive values for relative intensities of tin and indium peaks by numerical integration of the experimental data. These may be corrected for the ionization cross sections of the levels involved (*19, 20*) to yield the tin : indium ratios as sampled by the technique. Figure 3 illustrates the resulting ratios for samples containing 6 at.% Sn. Results for other compositions showed qualitatively similar variations. Ratios determined from Auger peaks, although showing the same general trends, are not included. This is because the weak In : 3*s* peak at 428 eV kinetic energy lies between the Sn and In Auger peaks and may be contributing to the integrated Sn peak intensity. Similarly, the Sn : $3p_{1/2}$ peak is not used as this coincides with the oxygen Auger peak at 511 eV kinetic energy.

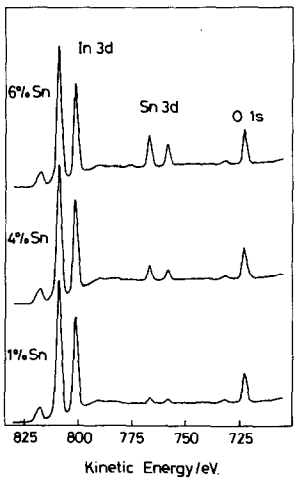

FIG. 1. Examples of Mg$K\alpha$ XPS of ITO ceramics fired at 1270 K in the metal 3*d* region. Peaks to the left of the main features are due to satellite radiation.

The tin : indium ratio at the surface of the pellets as sampled by XPS increases with

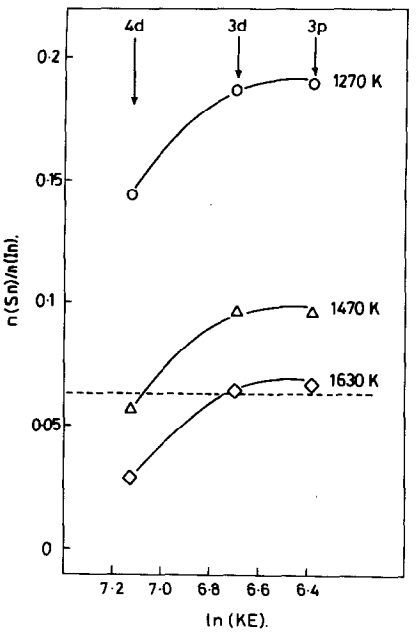

FIG. 3. The experimental tin : indium ratios, n(Sn)/n(In), determined from comparison of the tin and indium 4*d*, 3*d*, and 3*p* peaks plotted as a function of ln(electron kinetic energy) for samples containing nominally 6 at.% Sn. The dashed line indicates the nominal comparison. The solid lines are for heuristic purposes only.

nominal tin concentration, but decreases as the final firing temperature of the pellet is raised. Most of the data (with the exception of those for pellets fired at 1630 K taken from the 4*d* peaks—see below) indicate significant surface tin enrichment.

The tin : indium ratio as sampled by electrons in different kinetic energy ranges (i.e., having differing penetration depths, λ) is not the same and tends to increase with decrease in KE and thus in λ. This variation would not be expected if there were a thick tin-rich surface "phase"; if this were the case then electron energy-dependent variations in photoelectron mean-free-path length could not influence XPS intensity ratios. The observations suggest instead that segregation must be restricted to a layer at the surface which is thin compared with the electron mean-free-path (~10 Å). This hypothesis is supported by the observation that there is a rapid decrease in the tin : indium intensity ratio upon argon-ion etching the samples under mild conditions. Such an effect has also been reported by other authors (*13, 15*). Evidence from HREELS and UPS that the conduction electron concentration very near the surface is not higher than the nominal doping level (see Sections 3.2 and 3.3) appears to further exclude the possibility of a thick tin-rich layer.

An apparent anomaly in the results is seen for samples fired at 1630 K. Here the tin : indium ratio as determined from the 4*d* peaks is appreciably less than the bulk doping level. This would appear to indicate a depletion in tin at depths sampled by electrons in the higher KE range, having path lengths of around 15 Å. This is reinforced by the almost complete disappearance of the tin signals in the XPS spectra upon mild argon-ion etching of these samples.

The model for the surface therefore adopted for a detailed interpretation of the XPS data is one in which tin enrichment is restricted to the topmost ionic layer, which overlies a region having a tin content equal to or less than the bulk nominal content. If a fraction θ of the surface cation sites is occupied by tin, then (ignoring the small contribution to the photoelectron flux from tin ions in the bulk) the intensity ratio between tin and indium signals is given by

$$\frac{I_{Sn}}{I_{In}} = \frac{\sigma_{Sn}}{\sigma_{In}} \frac{\{1 - \exp(-D/\lambda)\}}{\{(1 - \theta) + \theta \exp(-D/\lambda)\}}. \quad (1)$$

Here D is the separation (normal to the surface) between adjacent cation-containing planes, λ is the electron mean-free-path length, and the σ are the ionization cross sections for the relevant subshells. Assuming that the electron scattering that leads to photoelectron attenuation can be described using a bulk jellium model for the solid,

Leckey and co-workers (*21, 22*) have derived a simple expression relating the electron pathlength $\lambda(E)$ to the kinetic energy, E:

$$\lambda(E) = 1.8\bar{E}E^{3/4}/E_p^2 \qquad (2)$$

(all energies in eV). E_p is the plasmon energy characteristic of the valence electrons of the system. This is given by the expression

$$E_p = 28.8(\rho z/A)^{1/2} \quad \text{(eV)}, \qquad (3)$$

where ρ is the density, A is the molecular weight, and z is the number of valence electrons per formula unit. In Eq. (2), $\bar{E}$ is the centroid of the optical loss function $\mathrm{Im}(-1/\varepsilon)$. This can be approximated to

$$\bar{E} = E_p + E_g, \qquad (4)$$

where E_g is the gap between the valence and conduction bands. Assuming that O : 2*p*, O : 2*s*, and *In* : 4*d* electrons contribute to the valence electron plasmon, one has $E_p = 27.0$ eV, and with $E_g = 3.6$ eV (*23*) this gives $\bar{E} = 30.6$ eV. Values of λ calculated for various kinetic energies using Eq. (2) ranged from 9.0 (In : 3*p*, KE = 588 eV) to 15.7 Å (In : 4*d*, KE = 1236 eV).

Equation (1) may now be used to estimate surface tin occupancy, using empirical estimates of subshell ionization cross sections taken from the tabulation of Evans and co-workers (*19*). For a polycrystalline material there is some ambiguity in the choice of the intercationic separation normal to the surface. For simplicity, this is taken to be the interplanar spacing between cation-containing planes in the In_2O_3 structure along the [100] direction. In_2O_3 crystals have been shown to grow preferentially in the [100] and [111] directions (*23*), and ITO thin films tend to exhibit predominant ⟨100⟩ or ⟨111⟩ texture (*5*).

In view of the simplicity of the model used and the assumptions made, the resulting values of surface occupancy, obtained using data from the 4*d*, 3*d*, and 3*p* peaks, showed a good degree of consistency. The experimental errors involved (for example, in the integration of peak areas) and the uncertainties in certain parameters, such as ionization cross sections, mean that the results must be regarded as semiquantitative. However, the occupancy values enable us to make rough estimates of the enthalpy and entropy of segregation of tin to the surface of doped In_2O_3. Simple thermodynamics (*24*) leads to the following relationship between surface (s) and bulk (b) tin cation site occupancies:

$$\frac{\theta_s}{(1-\theta_s)} = \frac{\theta_b}{(1-\theta_b)}\exp(-\Delta G/RT)$$

$$= \frac{\theta_b}{(1-\theta_b)}\exp(\Delta S/R)\exp(-\Delta H/RT), \qquad (5)$$

where ΔG, ΔH, and ΔS are respectively the free energy, enthalpy, and entropy of segregation and T is the temperature. In this case the final firing temperature of the pellet is used, as it is assumed that an equilibrium is established during firing which is quenched on cooling the pellet. The average values of surface occupancy obtained for 4*d*, 3*d*, and 3*p* peaks for various compositions are used to plot Fig. 4, from which values of ΔH and ΔS may be obtained (from the gradient and intercept with the $y = 0$ axis, respectively). Data for the 6% sample fired at 1270 K are omitted as XRD results demonstrate that this sample contains of the order of 5% tin in the form of SnO_2, so the surface model used is no longer applicable here. The graph yields values for ΔH and ΔS of -39 kJ mole^{-1} and -8.5 J K^{-1} mole^{-1}, respectively. The value obtained for the heat of segregation is of a similar order to that previously obtained by the authors for the heat of segregation of Sb to the surface of SnO_2 ceramics (*25, 26*). Note that there is quite a significant entropy change (of the order of R).

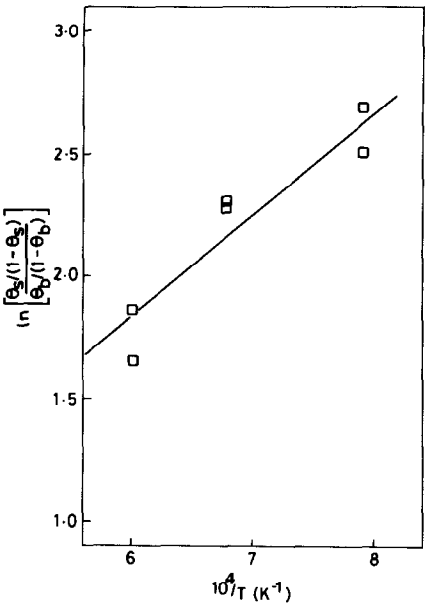

FIG. 4. ln(surface : bulk occupancy ratios) as a function of $1/T$ for ITO ceramics. The gradient of the line gives the heat of segregation of tin to the surface in accordance with Eq. (5).

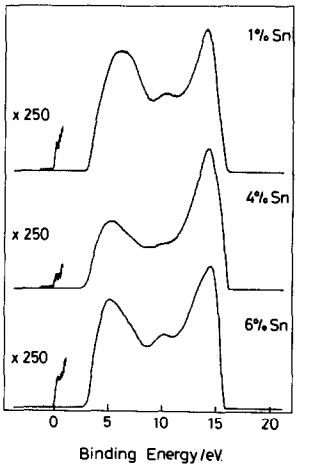

FIG. 5. HeI photoelectron spectra of ITO ceramics for various doping levels. All samples were fired at 1630 K. Binding energies are relative to the Fermi energy. The spectra have been stripped of structure due to HeIβ and HeIγ radiation.

3.2. Ultraviolet Photoelectron Spectroscopy

Ultraviolet photoelectron spectra excited with HeI ($h\nu$ = 21.2 eV) radiation over the composition range 1–6 at.% are shown in Fig. 5. The two dominant features of each spectrum are the filled valence band which has a sharp onset at about 3 eV below the Fermi energy and the strong secondary electron background with which it merges at about 10 eV below E_f. Tin doping appears to have little effect on the overall shape of the valence band, indicating that it is predominantly O : 2p in character.

On subtraction of structure due to HeIβ ($h\nu$ = 23.09 eV) and HeIγ ($h\nu$ = 23.75 eV) radiation from the raw spectra, a weak peak close to the Fermi energy is observed. This corresponds to conduction electrons introduced by tin doping. The band gap (measured from the base of the conduction band to the onset of the valence band) is approximately 2.5 eV, in accord with the value of the indirect band gap of 2.6 eV obtained by Weiher and Ley (*8*). The HeI photoelectron spectra represent an important direct measurement of the band structure of the material, which was recently reported as being unknown in most respects (*27*).

If each tin atom introduced by doping was contributing one electron to the conduction band of the material, one might expect the ratio of the intensity of the conduction band to that of the valence band to increase linearly with doping level. Subtraction of satellite structure allows this ratio to be measured, taking the conduction and valence bands to be defined by their respective high binding energy minima. Unfortunately the scatter in the ratio I(CB)/I(VB) is too large to allow for observation of well-defined trends with either doping level or calcining temperature. This is in contrast with behavior previously observed for ITO thin films, where data obtained using the Hall effect revealed a linear variation of free electron density with tin doping level for concentrations up to 5–6 at.% Sn

(*16*). Within the accuracy of the integration, the values obtained for the higher doping levels (where the integration is likely to be most successful) may be regarded as remaining roughly constant, giving a conduction band to valence band intensity ratio of around 7×10^{-5}.

The carrier concentration giving rise to this ratio may be estimated by using O : 2*p* and In : 5*s* matrix elements for ionization from valence and conduction bands, respectively. The bottom of the conduction band is expected to be predominantly In : 5*s*-like in character, justifying this assumption (*13*). Noting that there are eighteen O : 2*p* electrons and two In : 5*s* electrons per formula unit, we have

$$I(\mathrm{CB})/I(\mathrm{VB}) = 2x\sigma(\mathrm{In}:5s)/18\sigma(\mathrm{O}:2p), \quad (6)$$

where x is the fraction of tin atoms which have donated an electron to the conduction band. One-electron ionization cross sections were obtained from the calculations of Fadley *et al.* (*28*), giving

$$I(\mathrm{CB})/I(\mathrm{VB}) = 2.2 \times 10^{-5}n, \quad (7)$$

where n is the atomic percentage of tin contributing free carriers. Thus the ratio estimated for pellets containing 4 and 6 at.% Sn gives $n \sim 3.1$ at.%. The simple model used in Eq. (6) is likely to give a high value of n, as some of the more tightly bound valence states are not accessible to HeI UPS. Thus we may conclude that even in the samples containing 6 at.% Sn, the amount of substitutionally incorporated Sn is less than around 3 at.%.

3.3. *Electron Energy Loss Spectroscopy*

High-resolution electron energy loss spectra obtained with a 25-eV exciting electron beam are given in Fig. 6. This shows spectra for samples fired at 1470 K containing 1, 4, and 6 at.% Sn. Vibrational structure due to the excitation of surface optical phonons is seen immediately to the right of the elastic peak. However, the main feature of the spectra is a rather broader peak at an energy loss of approximately 0.5 eV for the 1% sample. This moves to progressively higher energy loss as the bulk tin content increases, and is due to excitation of the conduction electron surface plasmon. Overtones (due to multiple loss processes) are clearly visible in expanded scans of the spectra (Fig. 6).

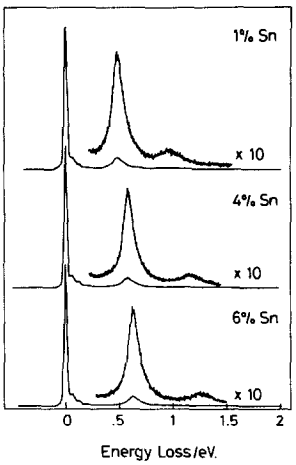

FIG. 6. HREEL spectra of ITO ceramics excited with a 25-eV electron beam. All samples were fired at 1470 K. FWHM ~50 meV.

The loss function $P(\omega)$ for scattering of low-energy electrons with velocity component v normal to the surface of a material with complex dielectric function $\varepsilon(\omega)$ is given by the expression (*29*)

$$P(\omega) = \frac{e^2}{vh\omega} \frac{\mathrm{Im}[\varepsilon(\omega) - 1]}{[\varepsilon(\omega) + 1]}. \quad (8)$$

Peaks in the loss spectra thus correspond to the condition

$$\mathrm{Re}(\varepsilon(\omega)) = -1 \quad (9)$$

(which differs from the *bulk* loss condition given by

$$\mathrm{Re}(e(\omega)) = 0). \quad (10)$$

For an array of damped oscillators with dynamic charge e, effective mass m^*, fre-

quency ω_0, and damping constant γ, the dielectric function $\varepsilon(\omega)$ is given by

$$\varepsilon(\omega) = \varepsilon_\infty + ne^2/m^*\varepsilon_0(\omega_0^2 - \omega^2 + i\omega\gamma), \quad (11)$$

where n is the concentration of oscillators, ε_0 is the permittivity of free space, and ε_∞ is the background dielectric constant. Local field corrections are omitted, since these vanish in the metallic regime (*30*). As the damping constant for plasmon oscillations is generally small, we may write

$$\varepsilon(\omega) = \varepsilon_\infty + ne^2/m^*\varepsilon_0(\omega_0^2 - \omega^2). \quad (12)$$

When $\omega = 0$, this reduces to the Drude dielectric function for a free-electron gas. Equating (12) to the loss condition (9) we obtain

$$(\omega_{sp}^2 - \omega_0^2) = ne^2/\varepsilon_0(\varepsilon_\infty + 1)m^*, \quad (13)$$

where ω_{sp} is the surface plasmon frequency. Thus, in the case where all incorporated tin is electrically active, the square of the plasmon frequency should vary linearly with nominal doping level. This type of behavior for the bulk plasmon has been observed in ITO thin films doped with up to around 5 at.% Sn (*2, 16*).

Table II shows the surface plasmon frequencies obtained for all the ceramic samples studied. The plasmon frequency increases with increasing doping level for all firing temperatures, but clearly by much smaller amounts than would be expected if each incorporated tin atom were contributing one electron to the conduction band of the sample.

Equation (13) may be used to estimate the free-carrier concentration giving rise to the observed plasmon frequency. Values of the high-frequency dielectric constant $\varepsilon_\infty = 4$ and electron effective mass $m^* = 0.35m_e$ are taken from the work of Köstlin *et al.* (*2, 16*). The resulting concentrations are shown in Table II, which also gives their equivalents in at.% Sn. For comparison purposes, the percentage of tin in the form of tin dioxide in each pellet as determined by XRD is shown.

The results indicate that at a dopant concentration of 1%, tin is substitutionally incorporated into the In_2O_3 lattice, each tin atom donating one electron to the conduction band of the sample. However, at higher doping levels this is not the case, as the free-carrier tin concentrations for most samples attain values only slightly over 1

TABLE II

PLASMON FREQUENCIES AND RESULTING FREE-CARRIER CONCENTRATIONS FOR ITO CERAMICS AS DETERMINED BY HREELS

Sn content (at.%)	Firing temperature (K)	Plasmon frequency, ω_{sp} (eV)	n (10^{21} cm^{-3})	n (at.% Sn)	SnO_2 content (at.% Sn)	"Residual" Sn content (at.%)
1	1270	0.485	0.298	0.96	0	0
	1470	0.477	0.289	0.93	0	0
	1630	0.472	0.283	0.91	0	0
4	1270	0.525	0.350	1.21	1–2	1
	1470	0.577	0.422	1.36	1–1.5	1
	1630	0.580	0.427	1.37	0	2.5
6	1270	0.535	0.363	1.17	5–6	0
	1470	0.625	0.496	1.59	2–3.5	2.5–1
	1630	0.605	0.464	1.49	0	4.5

at.%. These results are likely to be more accurate than those from UPS because the plasmon frequencies may be accurately measured and the analysis used involves fewer assumptions. Thus these results are fully consistent with those from UPS in that they demonstrate that the free-carrier concentration at the sampling depth of the technique is markedly less than the nominal tin content for samples containing 4 and 6 at.% Sn. Moreover, for these samples, it can be seen that there is generally a shortfall between the nominal doping level and the sum of the SnO_2 content and the tin substitutionally incorporated as sampled by HREELS. An estimate of this "residual" tin content is given in Table II.

4. Discussion

The conduction band to valence band intensity ratio in UPS and plasmon frequency in HREELS are both consistent with a concentration of electrons in the In : 5*s* conduction band that is significantly lower than the bulk nominal value for samples containing 4 and 6 at.% Sn. However, XPS results demonstrate that there is pronounced surface segregation of tin in the ceramic samples. The effective sampling depth in photoelectron spectroscopy is determined by the electron pathlength in the relevant kinetic energy regime, the latter being around 5–10 Å for UPS and 10–15 Å for XPS. The penetration depth of the surface plasmon in HREELS is given by v/ω and is about 30 Å using a 25-eV beam to probe a 0.5-eV excitation.

These considerations lead us to conclude that tin enrichment does not arise from a surface "phase" which is thick compared with the sampling depths of UPS, XPS, and HREELS. If this were the case, then each tin ion in a regular cation site in the In_2O_3 lattice would be expected to donate one electron to the conduction band, giving a surface free-carrier concentration much higher than that found experimentally. The fact that the tin : indium ratio from XPS spectra in different kinetic energy ranges is not constant confirms this and also eliminates the possibility of surface segregation of the bulk tin dioxide phase known to be present in some samples.

However, we may envisage that the asymmetric environment of the cations in the topmost surface plane will lead to a strong *s–p* hybridization, splitting off a local lone-pair-like surface state from the bulk conduction band (*25*). Thus, provided segregation is restricted to the topmost cation plane, segregated tin ions do not contribute electrons to the conduction band. The flexibility in oxygen content in the bixbyite structure would allow for the accommodation of Sn(II) ions at the surface of the material without the development of a surface charge.

Results from HREELS and UPS indicate that both techniques are probing a layer having a free-carrier concentration lower than the bulk nominal doping level in most cases. This could be attributable to either a reduction in tin concentration in this layer or trapping of bulk free carriers. The latter effect, due to introduction of oxygen during preparation, has been observed in studies on ITO thin films and may be reversed by annealing the films in a reducing atmosphere or *in vacuo* (*2–4, 16*). In this case we may suppose that defect "clusters" involving-interstitial oxygen, of the type proposed by Köstlin *et al.* (*4*) ((Sn_2O_i''), $(Sn_2O_4)^x$), may be present. However, we must note that the ceramic samples were subjected to high-temperature vacuum annealing overnight in order to produce spectroscopically clean samples and exhibited low free-carrier concentrations despite this treatment. Thus it appears that trapping is not the sole effect determining the carrier concentrations sampled, and that in addition there may exist a surface region of low tin concentration having a thickness at least of the

order of the penetration depth of HREELS, i.e. ~30 Å. The presence of such a layer, beneath the topmost layer of high tin concentration, is consistent with results obtained from XPS. Such a layer might possibly be created if, as the sample heating temperature is raised, some slight evaporation of tin from the surface occurs. In this case, superimposed on the segregation occurring in the equilibrated samples would be a dynamic effect due to the evaporation, resulting in a loss of tin in the layers close to the surface. In accordance, with this, the discrepancy between the carrier concentration given by HREELS and the nominal doping level is greatest at the highest calcining temperature, although TEM studies show that such evaporation does not significantly alter the overall stoichiometry. Band bending effects near the surface resulting from segregated tin may also contribute to the reduction in free carriers, although the observation of a conduction band in UPS indicates that a layer completely depleted in electrons (as in usually envisaged in such cases) cannot be present. Thus it seems possible that the low free-carrier concentration observed may be due to a complex combination of evaporation effects, band bending, and donor trapping effects.

Acknowledgments

The equipment used was funded by the SERC. W.R.F. is an SERC Postdoctoral Fellow.

References

1. J. C. C. Fan and F. J. Bachner, *J. Electrochem. Soc.* **122,** 1719 (1975).
2. H. Köstlin, *Festkörperprobleme* **22,** 229 (1982).
3. G. Frank, H. Köstlin, and A. Rabenau, *Phys. Status Solidi A* **52,** 231 (1979).
4. G. Frank and H. Köstlin, *Appl. Phys. A* **27,** 197 (1982).
5. Z. M. Jarzebski, *Phys. Status Solidi A* **71,** 13 (1982).
6. G. Rupprecht, *Z. Phys.* **139,** 504 (1954).
7. E. Kauer and R. Rabenau, *Z. Naturforsch.* **13,** 533 (1958).
8. R. L. Weiher and R. P. Ley, *J. Appl. Phys.* **37,** 299 (1966).
9. J. H. W. de Wit, *J. Solid State Chem.* **20,** 143 (1977).
10. J. H. W. de Wit, G. van Unen, and M. Lahey, *J. Phys. Chem. Solids* **38,** 819 (1977).
11. M. Hecq, A. Dubois, and J. van Cakenberghe, *Thin Solid Films* **18,** 117 (1973).
12. J. R. Bosnell and R. Waghorne, *Thin Solid Films* **15,** 141 (1973).
13. J. C. C. Fan and J. B. Goodenough, *J. Appl. Phys.* **48,** 3524 (1977).
14. K. D. J. Christian and S. R. Shatynski, *Thin Solid Films* **108,** 319 (1983).
15. N. R. Armstrong, A. W. C. Lin, M. Fujihira, and T. Kuwana, *Anal. Chem.* **48,** 741 (1976).
16. H. Köstlin, R. Jost, and W. Lems, *Phys. Status Solidi A* **29,** 87 (1975).
17. W. B. White and V. G. Keramidas, *Spectrochim. Acta, Part A* **28,** 501 (1972).
18. N. Beatham and A. F. Orchard, *J. Electron Spectrosc. Relat. Phenom.* **9,** 129 (1976).
19. S. Evans, R. G. Pritchard, and J. M. Thomas, *J. Electron Spectrosc. Relat. Phenom.* **14,** 341 (1978).
20. D. S. Urch and M. J. S. Urch, "ESCA(Mg)—Auger Table," supplied by V.G. Scientific, East Grinstead, UK (1981).
21. J. Szajman and R. C. G. Leckey, *J. Electron Spectrosc. Relat. Phenom.* **23,** 83 (1981).
22. J. Szajman, J. Leisegang, J. G. Jenkin, and R. C. G. Leckey, *J. Electron Spectrosc. Relat. Phenom.* **23,** 97 (1981).
23. R. L. Weiher, *J. Appl. Phys.* **33,** 2864 (1962).
24. G. A. Somorjai, "Chemistry in Two Dimensions: Surfaces," Chap. 3, Cornell Univ. Press, Ithaca, NY (1981).
25. R. G. Egdell, W. R. Flavell, and P. J. Tavener, *J. Solid State Chem.* **51,** 345 (1984).
26. P. A. Cox, R. G. Egdell, C. Harding, W. R. Patterson, and P. J. Tavener, *Surf. Sci.* **123,** 179 (1982).
27. I. Hamberg, C. G. Granqvist, K. -F. Berggren, B. E. Sernelius, and L. Engstrom, *Phys. Rev. B* **30,** 3240 (1984).
28. S. M. Goldberg, C. S. Fadley, and S. Kono, *J. Electron Spectrosc. Relat. Phenom.* **21,** 285 (1981).
29. G. D. Mahan, *in* "Elementary Excitations in Solids, Molecules and Atoms: Part B" (J. T. Devreese, A. B. Kunz, and T. C. Collins, Eds.), p. 93, Plenum, New York (1974).
30. P. A. Cox, *Solid State Commun.* **45,** 91 (1983).